Synthesis of $LiNi_{0.5}Mn_{0.5-x}Ti_xO_2$ by an Emulsion Drying Method and Effect of Ti on Structure and Electrochemical Properties

Seung-Taek Myung,† Shinichi Komaba,* Kiyoharu Hosoya, Norimitsu Hirosaki, Yusuke Miura, and Naoaki Kumagai

Department of Frontier Materials and Functional Engineering, Graduate School of Engineering, Iwate University, 4-3-5 Ueda, Morioka, Iwate 020-8551, Japan

Received January 6, 2005. Revised Manuscript Received February 27, 2005

Layered $LiNi_{0.5}Mn_{0.5-x}Ti_xO_2$ was prepared by an emulsion drying method. Solid solution of $LiNi_{0.5}Mn_{0.5-x}Ti_xO_2$ (*R*3*m*, space group) was formed to $x \leq 0.3$, and when $x > 0.3$, the layered structure transformed to the simple cubic structure. Rietveld refinement of X-ray diffraction data clearly showed that a small amount of Ti doping into $LiNi_{0.5}Mn_{0.5}O_2$ structure resulted in reduced cation mixing in the Li layer, and the stronger Ti−O bond relative to the Mn−O one would stabilize the crystal structure. Consequently, charge−discharge capacity and Li^+ chemical diffusion of $Li/LiNi_{0.5}Mn_{0.5-x}Ti_xO_2$ cells were enhanced by the improvement of physical properties in the oxide matrix. For a higher level of Ti doping, the obtained capacity decreased because a large amount of electro-inactive Ti^{4+} (d^0) depressed the conduction of electrons in the oxide. The cyclability of $Li/LiNi_{0.5}Mn_{0.5-x}Ti_xO_2$ ($x = 0-0.3$) cells was also dependent on the amount of Ti because of a different degree of cation mixing. In situ XRD observation confirmed that the variation in *c*-axis was different by increasing the Ti doping amount. That is, the Ti doping resulted in a smaller variation in the *c*-axis, which would be ascribed to the improvement of structural integrity by the stronger bond of Ti−O in the oxide matrix, compared to the Ti-free one. The Ti-doped $LiNi_{0.5}Mn_{0.5-x}Ti_xO_2$ materials also have good thermal safety characteristics at a highly oxidized state, as confirmed by differential scanning calorimetry.

Introduction

Lithiated cobalt oxide, $LiCoO_2$, is one of the most popular positive electrode materials in Li-ion secondary battery systems.[1] Fundamentally, the $LiCoO_2$ shows a high capacity with good reversibility when it is cycled between 2.0 and 4.3 V. Due to the dissolution of Co ingredient into the electrolyte accompanied by releasing oxygen from the host structure at a highly oxidized state, this material has a limited upper voltage cutoff to 4.3 V versus Li.[2,3]

$LiCoO_2$ is still relatively expensive and toxic. Therefore, it is likely that the better way is direct preparation of electrochemically stable positive electrode material such as $LiNi^{II}_{0.5}Mn^{IV}_{0.5}O_2$.[4,5] This material adopts a hexagonal unit cell like $LiCoO_2$ and $LiNiO_2$. In addition, it shows the superior characteristics of a larger capacity than $LiMn_2O_4$ and better thermal stability than $LiNiO_2$.[6,7] Recently, it was experimentally demonstrated that divalent Ni is oxidized to 4+ while tetravalent Mn remains inactive.[8,9] On the other hand, the tetravalent Mn provides significant structural stability during electrochemical cycling even at the high voltage cutoff limit, 4.6 V.

Kobayashi et al.[10,11] reported that $LiNi_{0.5}Mn_{0.5}O_2$ also shows cation mixing of about 10% due to the similarity of ionic radius between Li^+ and Ni^{2+}. Kang et al.[12] and our group[13] showed that discharge capacity of $LiNi_{0.5}Mn_{0.5}O_2$ was increased by 10−30% of its initial discharge capacity by doping with other elements, such as Al and Ti, and the cycling stability as well. However, the Al doping resulted in a significant increase in resistance of the oxide as measured by area specific impedance. Kim and Amine[14,15] also reported that an appropriate amount of Ti doping in $LiNiO_2$ enhances structural integrity, and it, in turn, provided improvement in cyclability. In some cases, though a small amount of Ti was introduced into $LiNiO_2$, the corresponding structural integrity and cyclability were even worse.[16,17] It is thought that such

* Corresponding author. Phone: +81 19 621 6329. Fax: +81 19 621 6328. E-mail: komaba@iwate-u.ac.jp.

† Current address: VK Corporation, 67 Jije-Dong, Pyongtaek-City, Kyonggi-Do 450-090, South Korea.

(1) Mizushima, K.; Jones, P. C.; Wiseman, P. J.; Goodenough, J. B. *Mater. Res. Bull.* **1980**, *15*, 783.
(2) Amatucci, G. G.; Tarascon, J. M.; Klein, L. C. *Solid State Ionics* **1996**, *83*, 167.
(3) Myung, S.-T.; Kumagai, N.; Komaba, S.; Chung, H.-T. *Solid State Ionics* **2001**, *139*, 47.
(4) Ohzuku, T.; Makimura, Y. *Chem. Lett.* **2001**, *2001*, 744.
(5) Lu, Z.; Beaulieu, L. Y.; Donaberger, R. A.; Thomas, C. L.; Dahn, J. R. *J. Electrochem. Soc.* **2002**, *149*, A778.
(6) Delmas, C.; Saadoune, I. *Solid State Ionics* **1992**, *53−56*, 370.
(7) Thackeray, M. M. *J. Electrochem. Soc.* **1995**, *142*, 2558.
(8) Yoon, W.-S.; Grey, C. P.; Balasubramanian, M.; Yang, X.-Q.; McBreen, J. *Chem. Mater.* **2003**, *15*, 3161.
(9) Yoon, W.-S.; Balasubramanian, M.; Yang, X.-Q.; Fu, Z.; Fischer, D. A.; McBreen, J. *J. Electrochem. Soc.* **2004**, *151*, 246.
(10) Kobayashi, H.; Sakaebe, H.; Kageyama, H.; Tatsumi, K.; Arachi, Y.; Kamiyama, T. *J. Mater. Chem.* **2003**, *13*, 590.
(11) Arachi, Y.; Kobayashi, H.; Emura, S.; Nakata, Y.; Tanaka, M.; Asai, T. *Chem. Lett.* **2003**, *32*, 60.
(12) Kang, S.-H.; Kim, J.; Stoll, M. E.; Abraham, D.; Sun, Y.-K.; Amine, K. *J. Power Sources* **2002**, *112*, 41.
(13) Myung, S.-T.; Komaba, S.; Hirosaki, N.; Hosoya, K.; Kumagai, N. *J. Power Sources*, in press.
(14) Kim, J.; Amine, K. *Electrochem. Commun.* **2001**, *3*, 52.
(15) Kim, J.; Amine, K. *J. Power Sources* **2002**, *104*, 33.
(16) Chang, S. H.; Kang, S.-G.; Song, S.-W.; Yoon, J.-B.; Choy, J.-H. *Solid State Ionics* **1996**, *86−88*, 171.

10.1021/cm050033j CCC: $30.25
Published on Web 03/30/2005

a difference may be caused by an inappropriate synthetic method. Noguchi's group recently suggested that a favorable way to prepare Ti-doped cathode material is to use the solution method instead of the conventional solid-state route.[18−20]

In this work, layered $LiNi_{0.5}Mn_{0.5-x}Ti_xO_2$ ($x = 0-0.3$) was successfully synthesized via an emulsion drying method, which gives an ultimate homogeneous powder precursor.[21] We report on our investigation of Ti doping effects on structure and electrochemical properties of $LiNi_{0.5}Mn_{0.5-x}Ti_xO_2$.

Experimental Section

$LiNi_{0.5}Mn_{0.5-x}Ti_xO_2$ powders were prepared by the emulsion drying method. We previously reported details of the emulsion drying method.[21−23] Starting materials used for the synthesis of $LiNi_{0.5}Mn_{0.5-x}Ti_xO_2$ were $LiNO_3$ (Kanto), $Mn(NO_3)_2{\cdot}6H_2O$ (Kanto), $Ni(NO_3)_2{\cdot}6H_2O$ (Kanto), and $Ti[OCH(CH_3)_2]_4$ (Aldrich). In the starting emulsion, the atomic ratio of Li/(Ni+Mn+Ti) and Ni/(Mn+Ti) were 1.25 and 1, respectively. The obtained powder precursors were preliminarily annealed at 400 °C for 6 h in air, and then they were calcined at 950 °C for 12 h in air.

X-ray diffractometry (XRD, Rigaku Rint 2200) and transmission electron microscopy equipped with energy-dispersive spectroscopic (EDX) elemental mapping (TEM; 200 kV, Hitachi, H-800) were employed to characterize the prepared powders. XRD data were obtained $2\theta = 10$ to 100°, with a step size of 0.03° and a count time of 5 s. The collected intensity data of XRD were analyzed by the Rietveld refinement program, *Fullprof* 2000.[24] Chemical compositions of the resulting powders were analyzed by atomic absorption spectroscopy (Analyst 300, Perkin-Elmer).

For fabrication of working electrodes, the prepared powders were mixed with acetylene black and polyvinylidene fluoride (80:15:5 in weight) in *N*-methylpyrrolidinon. The slurry thus obtained was coated onto Al foil and dried at 80 °C for 1 day for roll-pressing (500 kg cm^{-2}). The cathode loading was about 10 mg onto the Al disk after punching (16 mm in diameter). The electrodes were dried again at 120 °C for 4 days in a vacuum state prior to use. A 2032 type of coin cell consisted of the cathode, lithium foil as an anode, and 1 M $LiPF_6$ in ethylene carbonate−diethyl carbonate (2:1 in volume) as an electrolyte. The cells were charged and discharged between 2.7 and 4.6 V vs Li by applying a current density of 20 mA g^{-1} at 25 °C. For galvanostatic intermittent titration technique (GITT) measurement, a constant current flux was applied for a given time followed by open circuit for 10 h.

In situ XRD data were obtained using a Rigaku Rint 2200 diffractometer from $2\theta = 10$ to 70°, with a step size of 0.03° and a count time of 7 s. The in situ cell and attachment were fabricated by Rigaku, Inc., with a polypropylene film window fitted in the base of the cell to avoid the corrosion of a conventional beryllium window at higher potentials. The cell was charged and discharged with a current density of 20 mA g^{-1}. The lattice parameters were calculated by the following method: the positions of the individual peaks were fitted with a psuedo-Voigt or Lorentz function, and typically 10 or 12 peak positions were inputted to minimize the least-squares difference between the calculated and measured peak positions by adjusting the lattice constant and the vertical displacement of the sample.

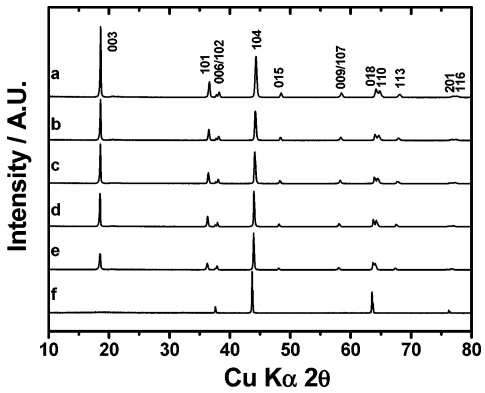

Figure 1. XRD patterns of $LiNi_{0.5}Mn_{0.5-x}Ti_xO_2$ calcined at 950 °C for 12 h in air: (a) $x = 0$, (b) $x = 0.05$, (c) $x = 0.1$, (d) $x = 0.2$, (e) $x = 0.3$, and (f) $x = 0.5$.

Table 1. Chemical Compositions of $LiNi_{0.5}Mn_{0.5-x}Ti_xO_2$ Calcined at 950 °C for 12 h in Air Measured by AAS

x in $LiNi_{0.5}Mn_{0.5-x}Ti_xO_2$	chemical compositions	color
0	$Li_{1.00}Ni_{0.48}Mn_{0.50}O_2$	black
0.05	$Li_{1.01}Ni_{0.49}Mn_{0.45}Ti_{0.05}O_2$	black
0.1	$Li_{1.00}Ni_{0.49}Mn_{0.40}Ti_{0.10}O_2$	black
0.2	$Li_{1.02}Ni_{0.48}Mn_{0.30}Ti_{0.19}O_2$	dark brown
0.3	$Li_{0.98}Ni_{0.48}Mn_{0.20}Ti_{0.29}O_2$	dark brown
0.5		yellow green

For differential scanning calorimetry (DSC) experiments, the cells were finally charged to 4.6 V and opened in the Ar-filled drybox. After the cell was carefully opened in the Ar-filled drybox, the extra electrolyte was removed from the surface of the electrode, and the electrode materials were recovered from the current collector. A stainless steel-sealed pan with a gold-plated copper seal (which can withstand 150 atm of pressure before rupturing and has a capacity of 30 μL) was used to collect 3−5 mg samples. The measurements were carried out in a Pyris 1 differential scanning calorimeter (Perkin-Elmer) using a temperature scan rate of 1 °C min^{-1}. The weight was constant in all cases, indicating that there were no leaks during the experiments.

Results and Discussion

Figure 1 shows XRD patterns of $LiNi_{0.5}Mn_{0.5-x}Ti_xO_2$ ($x = 0-0.5$), obtained by calcining the emulsion-dried powders at 950 °C for 12 h in air. The starting ratio of Li/[Ni+Mn] was decided to be 1.25 because a small amount of lithium evaporation was observed at higher temperature; furthermore, prolonged heat treatment at that temperature resulted in much more evaporation of lithium.[25] Therefore, calcination of the emulsion-dried powder (Li/[Ni+Mn+Ti] = 1.25) at 950 °C for 12 h in air brought about stoichiometric compositions as analyzed by atomic absorption spectroscopy (AAS), as shown in Table 1. The diffraction patterns can be identified as a hexagonal α-$NaFeO_2$ structure with space group $R\bar{3}m$ up to $x = 0.3$ in $LiNi_{0.5}Mn_{0.5-x}Ti_xO_2$. For $x = 0.5$ in $LiNi_{0.5}Mn_{0.5-x}Ti_xO_2$ the structure changed to a simple cubic structure (Figure 1f) because of the disappearance of

(17) Joeng, J. W.; Kang, S.-G. *J. Power Sources* **2003**, *123*, 75.
(18) Zhang, L.; Noguchi, H. *Electrochem. Commun.* **2002**, *4*, 560.
(19) Zhang, L.; Muta, T.; Noguchi, H.; Wang, X.; Zhou, M.; Yoshio, M. *J. Power Sources* **2003**, *117*, 137.
(20) Zhang, L.; Wang, X.; Noguchi, H.; Yoshio, M.; Takada, K.; Sasaki, T. *Electrochim. Acta* **2004**, *49*, 3305.
(21) Myung, S.-T.; Komaba, S.; Kumagai, N. *J. Electrochem. Soc.* **2001**, *148*, A482.
(22) Myung, S.-T.; Komaba, S.; Kumagai, N.; Yashiro, H.; Chung, H.-T.; Cho, T.-H. *Electrochim. Acta* **2002**, *47*, 2543.
(23) Myung, S.-T.; Komaba, S.; Hirosaki, N.; Kumagai, N.; Arai, K.; Kodama, R.; Nakai, I. *J. Electrochem. Soc.* **2003**, *150*, A1560.
(24) Roisnel, T.; Rodriguez-Carjaval, J. *Fullprof Manual*; Institut Laue-Langevin: Grenoble, 2000.
(25) Myung, S.-T.; Komaba, S.; Kumagai, N. *Solid State Ionics* **2004**, *170*, 139.

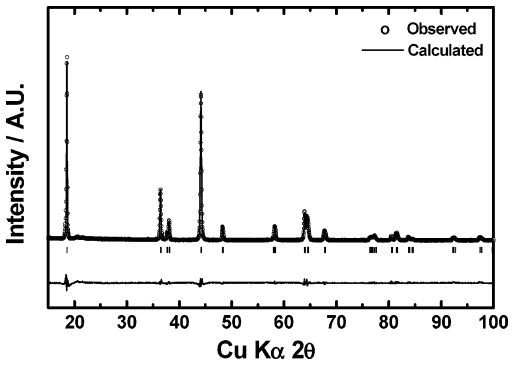

Figure 2. Rietveld refinement result of XRD pattern of $LiNi_{0.5}Mn_{0.4}Ti_{0.1}O_2$ calcined at 950 °C for 12 h in air.

the (003) peak. A clearer splitting of (108) and (110) is seen for $LiNi_{0.5}Mn_{0.5-x}Ti_xO_2$ ($x = 0-0.3$) in Figure 1, which indicates that the layered structure is developed well. Colors of the prepared powders were also dependent on the Ti substitution amount, as described in Table 1. A small amount of Ti substitution for Mn resulted in black color. However, a higher level of Ti replacement gave dark brown or green color, which is indicative of its low electronic conductivity as the similarity was reported by Tsuda et al.[26]

There are some striking features in the XRD patterns in Figure 1. First, the diffraction peaks are shifting to a lower angle with increasing amount of Ti, which indicates a gradual increase in lattice parameters. Second, the integrated intensity of the (003) peak is gradually decreased by increasing Ti doping amount (Figure 1a−e). The intensity becomes smaller than that of the (104) peak from $x = 0.2$ in $LiNi_{0.5}Mn_{0.5-x}Ti_xO_2$. In fact, the amount of the Li element is close to 1 as confirmed by AAS (Table 1). However, a small amount of the tetravalent Ti, whose valence is equivalent to that of Mn, resulted in such a decrease in (003) intensity, as shown in Figure 1. Third, full-width at half-maximum (fwhm) of the (104) peak decreased with increasing Ti doping amount.

To understand the influence of the Ti doping on the structure, Rietveld refinements were carried out for all compositions by assuming the space group of $R\bar{3}m$. For the refinements, it was supposed that Ni^{2+} located at the 3a sites can be exchanged with Li^+ occupied at the 3b site due to similarity of their ionic radii (Li^+: 0.70 Å; Ni^{2+}: 0.76 Å[27]). For Ti^{4+} (0.60 Å) and Mn^{4+} (0.54 Å) the ionic radii are much smaller than that of Li^+ so that the possibility of Ti^{4+} and Mn^{4+} incorporation into the Li layer is excluded for the refinement. The resultant refinement pattern and parameters are shown in Figure 2 and Tables 2 and 3, respectively. The refinements resulted in a good agreement between the observed and calculated patterns, shown in Figure 2. The lattice parameters were also calculated by the refinement as shown in Figure 3. The *a*- and *c*-axes increased linearly with Ti substitution, suggesting that Ti was substituted for the Mn, obeying Vegard's law. The reason for the increase in the structural parameter is primarily due to the difference in the ionic radius of Mn^{4+} (0.54 Å) and Ti^{4+} (0.60 Å). These results clearly confirm that Ti substitution for Mn sites was successful and the single-phase solid solution was formed up to $x = 0.3$ in $LiNi_{0.5}Mn_{0.5-x}Ti_xO_2$.

Cation mixing of the final products was greatly dependent on Ti amount (Figure 4). The Ti-free sample showed a high cation mixing ratio of about 10%, which usually appears in the literature.[10,11] As was reported previously by Chang et al.,[16] a small amount of Ti substitution for Ni in the $LiNiO_2$ system usually brought about a severe cation mixing. On the other hand, the cation mixing abruptly decreased by a small amount of Ti doping in the $LiNi_{0.5}Mn_{0.5}O_2$ structure in our

Table 2. Structural Parameters Obtained from Rietveld Refinement of XRD Data of $LiNi_{0.5}Mn_{0.4}Ti_{0.1}O_2$ Calcined at 950 °C for 12 h in Air (Starting Ratio of Li/M = 1.25)

formula		$LiNi_{0.5}Mn_{0.4}Ti_{0.1}O_2$			
crystal system		hexagonal			
space group		$R\bar{3}m$			
atom	site	*x*	*y*	*z*	*g*
Li	3a	0	0	1/2	0.933(5)
Ni	3a	0	0	1/2	0.062(5)
Li	3b	0	0	0	0.062
Ni	3b	0	0	0	0.436(4)
Mn	3b	0	0	0	0.394(4)
Ti	3b	0	0	0	0.098(4)
O	6c	0	0	0.2574(20)	1

Table 3. Metal−Oxygen Distances of $LiNi_{0.5}Mn_{0.5-x}Ti_xO_2$ Calcined at 950 °C for 12 h in Air[a]

x in $LiNi_{0.5}Mn_{0.5-x}Ti_xO_2$	Li−O (Å)	M−O (Å)	MO_2 (Å)	M−M (Å)	R_{wp} (%)
0	2.1045(11)	1.9812(11)	2.3143	4.7621	13.5
0.05	2.1084(18)	1.9880(16)	2.1581	4.7666	4.70
0.1	2.1111 (18)	1.9936(16)	2.1869	4.7709	5.83
0.2	2.1185(15)	1.9998(24)	2.1987	4.7777	6.14
0.3	2.1256(21)	2.0097(15)	2.2169	4.7843	14.7

[a] The distances were calculated by Rietveld refinement. (Average Li−O and M−O distances, thickness of the MO_2 slab layer and metal to metal (M−M) interlayer distances.) M donates Ni, Co, and Mn. $MO_2 = (2/3 - 2 \times z_{oxygen}) \times c$. M−M = $c/3$.

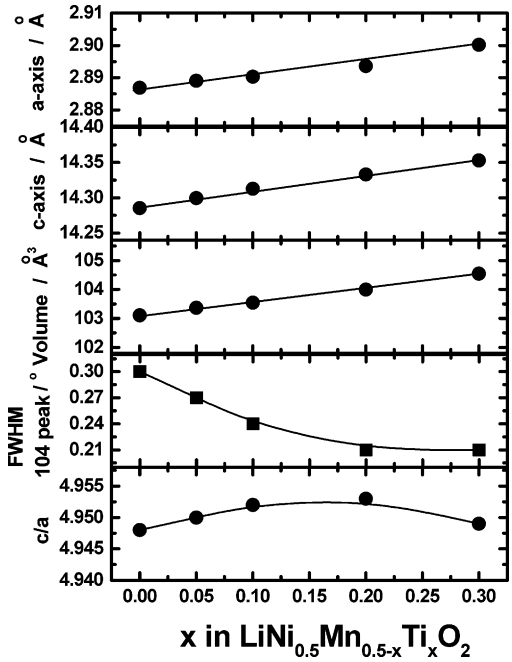

Figure 3. Variation of lattice parameters of $LiNi_{0.5}Mn_{0.5-x}Ti_xO_2$ ($x = 0-0.3$) calculated by Rietveld refinements.

(26) Tsuda, M.; Arai, H.; Ohtsuka, H.; Sakurai, Y. *Electrochem. Solid-State Lett.* **2004**, *7*, A343.
(27) Shannon, R. D. *Acta Crystallogr., Sect. A: Found. Crystallogr.* **1976**, *32*, 751.

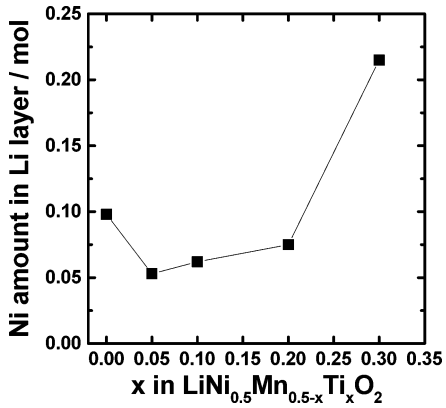

Figure 4. Ni amount in Li layer of $LiNi_{0.5}Mn_{0.5-x}Ti_xO_2$ ($x = 0-0.3$) obtained by Rietveld refinements.

experiment (Figure 4). When $x = 0.3$ in $LiNi_{0.5}Mn_{0.5-x}Ti_xO_2$, the cation mixing increased drastically again up to 23% probably due to the formation of solid solution of $LiTiO_2$ that showsed $I_{(003)}/I_{(104)} = 0.6$.[28] However, one can clearly observe the disappearance of the (003) peak for $x = 0.5$ in $LiNi_{0.5}Mn_{0.5-x}Ti_xO_2$ in Figure 1f, which shows simple cubic structure. In this case, the average oxidation state of Ti is 4+. This suggests the difficulty of the formation of rock-salt-structured $LiTiO_2$ in the final product, whose valence of Ti is 3+. As mentioned in Figure 1, Ti doping slightly lowers the integrated peak intensity of (003) peak. Nonetheless, the cation mixing is still lower until $x = 0.2$ than that of $x = 0$ in $LiNi_{0.5}Mn_{0.5-x}Ti_xO_2$ (Figure 2). As can be seen in Figure 1, the full-width at half-maximum of the (104) peak is clearly decreasing with incorporation of Ti into the $LiNi_{0.5}Mn_{0.5}O_2$ structure (Figure 3). It is more likely that the cation mixing would be related to bonding strength between metal ion and oxygen in this case because the amount of divalent Ni remains unchanged for all compositions as shown in Table 1, and the tetravalent Ti was partly substituted for the equivalent Mn. If the cation mixing occurs preferably depending on the ionic radius, the occurrence of the cation mixing should be much favored by Ti doping in the $LiNi_{0.5}Mn_{0.5}O_2$ structure because the ionic radius of Ti^{4+} is closer to Li^+, compared to Mn^{4+}. However, the result clearly indicates that the degree of cation mixing was reduced by a small amount of Ti substitution (Figure 4). Though a direct comparison is impossible due to the lack of information about the bonding strength, it is able to deduce by employing the Gibbs free energy of the formation at 298 K, i.e., MnO_2 (-465.14 kJ mol^{-1}) and TiO_2 (-889.5 kJ mol^{-1}).[29] Hence, Ti^{4+} substitution for Mn^{4+} indirectly means that the bonding strength of the oxide matrix by Ti doping is stronger than that of Ti-free $LiNi_{0.5}Mn_{0.5}O_2$. That is, the structural integrity of the oxide would be influenced by introduction of the strong bonding of Ti−O into the crystal structure. From the above results, it is suggested that a small amount of Ti doping is significantly effective in stabilizing the $LiNi_{0.5}Mn_{0.5-x}Ti_xO_2$ structure.

Figure 5 shows the STEM elemental analysis image and the corresponding EDS maps of Ni, Mn, and Ti for the $LiNi_{0.5}Mn_{0.2}Ti_{0.3}O_2$. The observed particle size was about 1 μm in diameter. Clearly, Ni, Mn, and Ti were uniformly distributed throughout the crystalline oxide, which coincides with the Rietveld refinement of XRD data. This indicated that the emulsion drying method made it possible and easy to form the solid solution oxides.

Figure 6 illustrates the cell voltage versus capacity curves for the first charge and discharge of $Li/LiNi_{0.5}Mn_{0.5-x}Ti_xO_2$ ($x = 0-0.3$) cells between 2.7 and 4.6 V. The cathodes are first galvanostatically charged and subsequently discharged by application of a current density of 20 mA g^{-1} at 25 °C. The Ti-free $LiNi_{0.5}Mn_{0.5-x}Ti_xO_2$ had the initial discharge capacity of 154 mA h g^{-1}, showing a Coulombic efficiency of 72%. However, the cathode doped with 0.05 mol of Ti per formula unit delivered an increased discharge capacity of 175 mA h g^{-1}, of which the efficiency corresponds to 77% (Figure 6). When $x = 0.3$ in $LiNi_{0.5}Mn_{0.5-x}Ti_xO_2$, the initial discharge capacity was only 88 mA h g^{-1} and the efficiency between charge and discharge capacity was only about 44%. Such a large irreversible capacity is probably due to the greater cation mixing into the Li layer at a higher level of Ti substitution; similar phenomena were observed by Delmas' group.[30,31] Furthermore, the polarization estimated between charge and discharge potentials was decreasing for $x = 0.05$ and 0.1 in $LiNi_{0.5}Mn_{0.5-x}Ti_xO_2$, but the polarization became higher by further increasing the Ti doping amount (in Figure 6). Such behaviors from the obtained capacity and polarization would be related to the cation mixing as is seen in Figure 4. If the divalent Ni ion is located at the 3b site (Li layer), it consequently disturbs the Li^+ diffusion in the interslab space with larger polarization. Therefore, $LiNi_{0.5}Mn_{0.5-x}Ti_xO_2$ ($x = 0.05-0.1$), possessing the lower cation mixing, exhibited lower polarization to enhance the electrochemical properties. Similar results were also seen in the same system, as reported by Noguchi's group.[32]

To observe the detailed difference by Ti substitution, the initial charge and discharge curves were differentiated as shown in Figure 7. The Ti doping up to $x = 0.1$ in $LiNi_{0.5}Mn_{0.5-x}Ti_xO_2$ slightly increased the charge and discharge voltage. Higher level of Ti doping brought about an increase in the operation voltage (Figure 7). Goodenough's group[33] explained a similar phenomenon using oxide and sulfide. We also explained a similar result for the oxide system $LiAl_xMn_{2-x}O_4$.[21] In these cases, the stronger bonding resulted in an increase in redox energy. As mentioned above in Figure 4, Ti−O bonding would be stronger than that of Mn−O so that the stronger bonding, in turn, would raise the redox potential of $Ni^{2+/4+}$ (Figure 7).

Figure 8 depicts the continuous charge and discharge curves of the $Li/LiNi_{0.5}Mn_{0.5-x}Ti_xO_2$ ($x = 0-0.3$) cells between 2.7 and 4.6 V by application of a current density of 20 mA g^{-1} at 25 °C. The Ti-free sample showed the initial

(28) *Joint Committee on Powder Diffraction Standards*, File No. 40-1053.
(29) Samsonov, G. V. *The Oxide Handbook*, 2nd ed.; IFI/Plenum Inc., USA, 1982; pp 44−48.
(30) Pouillerie, C.; Croguennec, L.; Biensan, Ph.; Willmann, P.; Delmas, C. *J. Electrochem. Soc.* **2000**, *147*, 2061.
(31) Gulimard, M.; Croguennec, L.; Delmas, C. *J. Electrochem. Soc.* **2003**, *150*, A1287.
(32) Li, D.; Muta, T.; Noguchi, H. *J. Power Sources* **2004**, *135*, 262.
(33) Manthiram, A.; Goodenough, J. B. *J. Solid State Chem.* **1987**, *71*, 349.

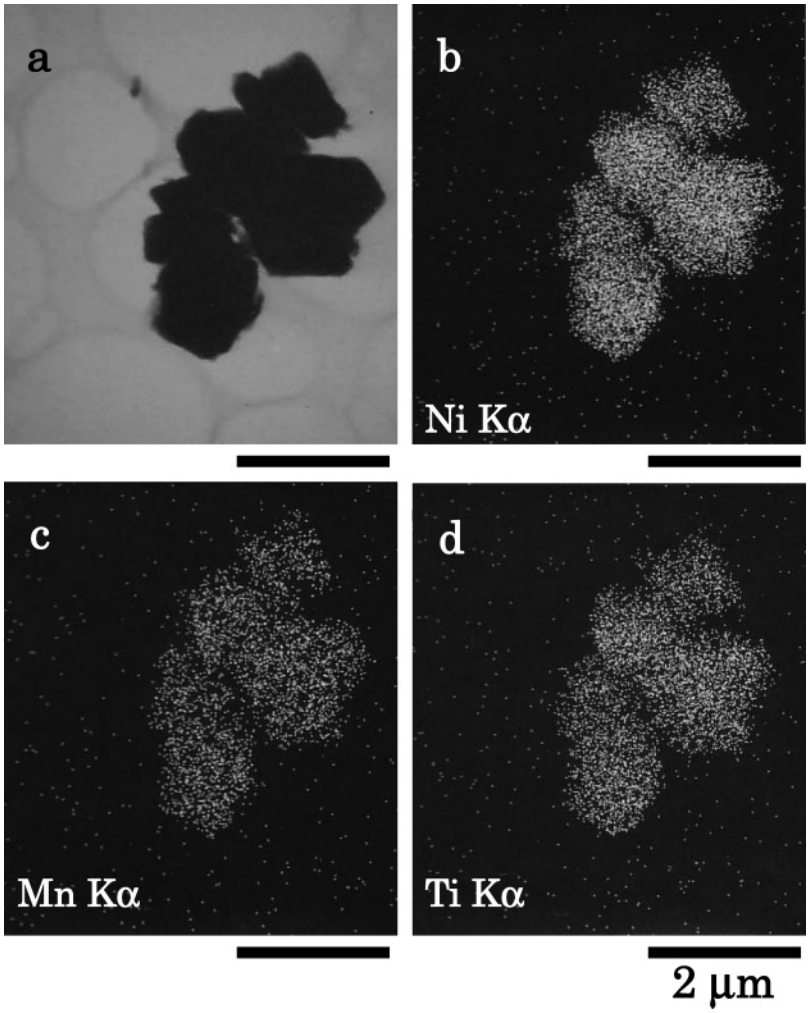

Figure 5. (a) STEM image of $LiNi_{0.5}Mn_{0.2}Ti_{0.3}O_2$ calcined at 950 °C for 12 h in air; EDS mappings of (b) Ni, (c) Mn, and (d) Ti elements.

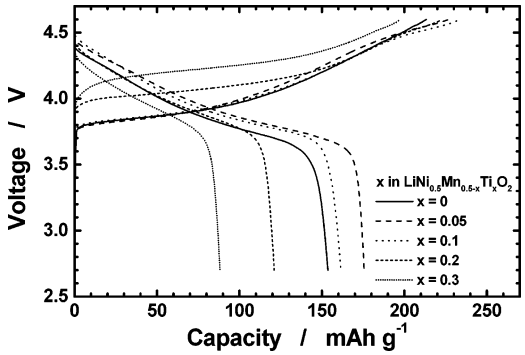

Figure 6. Initial charge and discharge curves of $Li/LiNi_{0.5}Mn_{0.5-x}Ti_xO_2$ ($x = 0-0.3$) cells. A constant current density of 20 mA g^{-1} was applied across the cathode between 2.7 and 4.6 V at 25 °C.

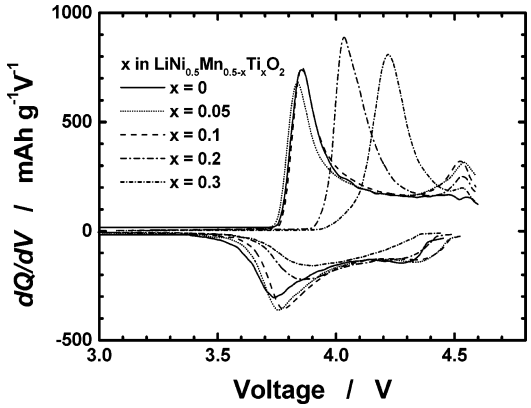

Figure 7. Differential capacity versus voltage of the initial charge and discharge curves for $Li/LiNi_{0.5}Mn_{0.5-x}Ti_xO_2$ ($x = 0-0.3$) cells.

discharge of about 154 mA h g^{-1} and retained its original capacity of 90% at the 50th cycle (in Figure 8a). As the Ti content increased up to $x = 0.1$, $Li/LiNi_{0.5}Mn_{0.5-x}Ti_xO_2$ cells exhibited some increased discharge capacities and capacity retention, compared to those of $LiNi_{0.5}Mn_{0.5}O_2$. Especially, when $x = 0.1$, the capacity retention at the 50th was close to 99% of its initial discharge capacity. Further Ti doping lowers the obtained discharge capacity in Figure 8d,e. This behavior can be understood by the following supposition: electrons produced by the oxidation reaction ($Ni^{2+} \rightarrow Ni^{4+} + 2e^-$) probably migrate through the d orbital in the transition metal layer. The octahedral site containing Ni^{2+} would be surrounded by octahedral sites containing Ti^{4+} (d^0) and Mn^{4+} (d^3). The large amount of Ti^{4+} (d^0) would block the current path, hence, the increased electronic resistance of the $LiNi_{0.5}Mn_{0.5-x}Ti_xO_2$ resulting in the lower capacity. As described in Table 1, the poor electronic conductivity would be one reason for this insufficient performance. From this consideration, the lower capacity of $LiNi_{0.5}Mn_{0.5-x}Ti_xO_2$ cells might be ascribed to the blocking of the electron conduction through the octahedral sites occupied by Ti^{4+} during electrochemical Li^+ de/-intercalation, especially under higher Ti concentration. The difficulty of the electron transport

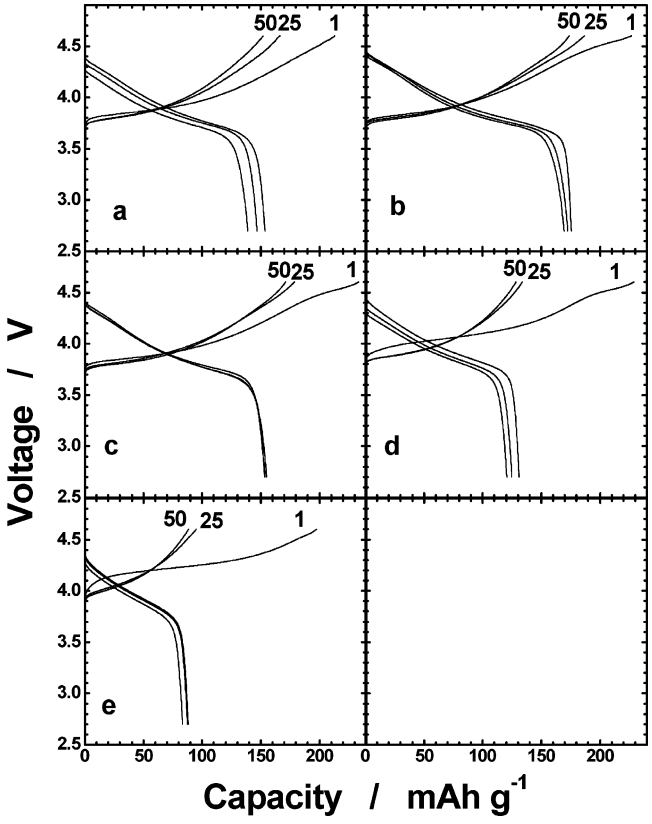

Figure 8. Continuous charge and discharge curves of $Li/LiNi_{0.5}Mn_{0.5-x}Ti_xO_2$ ($x = 0 - 0.3$) cells; (a) $x = 0$, (b) $x = 0.05$, (c) $x = 0.1$, (d) $x = 0.2$, and (e) $x = 0.3$. A constant current density of 20 mA g^{-1} was applied across the cathode between 2.7 and 4.6 V at 25 °C.

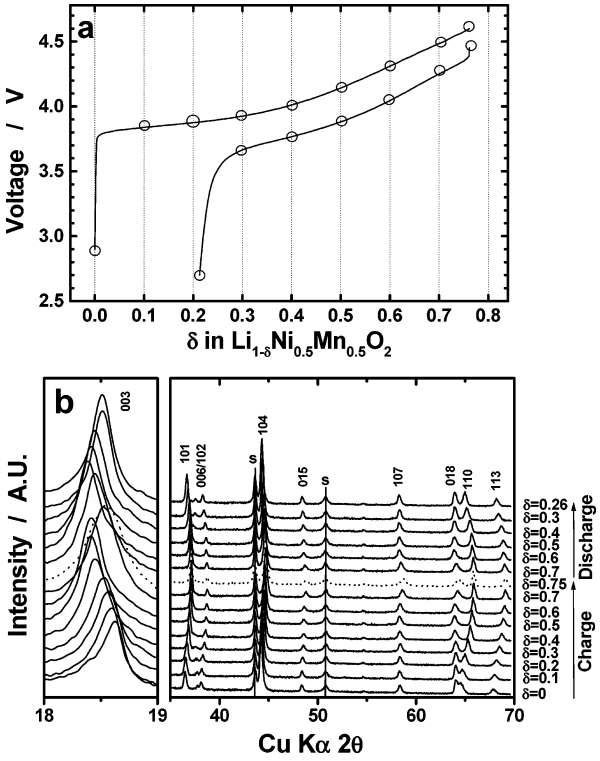

Figure 9. (a) Charge and discharge curves of the initial cycle for $Li/LiNi_{0.5}Mn_{0.5}O_2$ cell. In situ XRD measurements were carried out at the position marked by the circles. (b) In situ XRD patterns of $Li_{1-\delta}Ni_{0.5}Mn_{0.5}O_2$ as a function of Li content during the first cycle. S donates a stainless ex-met for loading active materials, and the ex-met was used as the internal standard for calibration.

consequently led to the large resistance as seen in Figures 6 and 7; similar phenomena were previously observed in the spinel $LiNi_{0.5}Mn_{1.5-x}Ti_xO_4$ system.[34] Accordingly, it was found that a small amount of Ti doping to $x = 0.1$ enhanced the obtainable discharge capacity because of the improvement in structural integrity, but higher Ti contents deteriorated the capacity due to the structural disorder by cation mixing and blocking of electron transport by an electro-inactive Ti ingredient.

In situ XRD measurements were carried out to understand structural changes of the active materials and their dependence on Ti contents. The first charge and discharge curves are given, and the measurements were done at the circle-marked points in Figures 9a, 10a, and 11a. Diffraction peaks of stainless ex-met (revealed as S) are used as the internal standard and the corresponding patterns are shown in Figures 9b, 10b, and 11b.

As Li^+ deintercalated from the host structure, (00*l*) peaks were gradually shifted toward a lower angle until δ is 0.6 in $Li_{1-\delta}Ni_{0.5}Mn_{0.5}O_2$ (Figure 9b). Then the peaks were moved to a higher angle in the first charge stage (Figure 9b). On the other hand, all other peaks were shifted smoothly toward a higher angle in 2θ during the first charge without any peaks of secondary phases in the XRD pattern. The reversible behaviors were seen during discharge. When δ is 0.4 in $Li_{1-\delta}Ni_{0.5}Mn_{0.5}O_2$, one can see minor changes in the diffraction pattern, that the (006) peak is merged with the (102) peak on charge (Figure 9b). For $Li_{1-\delta}Ni_{0.5}Mn_{0.45}Ti_{0.05}O_2$, similar behavior was observed at $\delta = 0.5$ in $Li_{1-\delta}Ni_{0.5}Mn_{0.45}Ti_{0.05}O_2$ on charge (Figure 10b), similar to $Li_{1-\delta}Ni_{0.5}Mn_{0.5}O_2$. Meanwhile, overlapping of (102) and (006) peaks was hardly observed for $Li_{1-\delta}Ni_{0.5}Mn_{0.2}Ti_{0.3}O_2$ (Figure 11b), which means that single-phase reaction occurred topotactically during Li^+ de-/intercalation.

From in situ XRD patterns in Figures 9−11, lattice parameters were calculated by the least-squares method and the results are shown in Figure 12. Differences in the *a*- and *c*-axes and unit volume (Δa, Δc, and ΔV, respectively) during the first cycle were used for comparison. The lattice parameters were calculated based on hexagonal lattice ($R\bar{3}m$). As Li^+ ions were extracted from the host structure, *a*-axis decreased monotonically, which corresponds to the reduction of the metal−metal interslab distance, because the ionic radii of Ni^{3+} and Ni^{4+} formed during charge are smaller than that of Ni^{2+}. This, therefore, leads to a decrease of metal−oxygen distance and increase in covalency, especially at the highly delithiated state. The reverse variations in the *a*-axis were seen upon the intercalation process. The *c*-axis constant increased until 0.5 mol of Li^+ per formula unit was extracted, and then the value of *c*-axis parameter decreased abruptly in the following deintercalation for $Li_{1-\delta}Ni_{0.5}Mn_{0.5-x}Ti_xO_2$ ($x = 0$, 0.05). The increase in the *c*-axis parameter is due to the increase in the Coulombic (electrostatic) repulsion force between the oxygen−oxygen layers by the ionicity of M−O bonding. And the decrease in the *c*-axis parameter in a highly oxidized state ($\delta > 0.5$) is probably due to less electrostatic repulsion between the oxygen−oxygen layers resulting from

(34) Kim, J.-H.; Myung, S.-T.; Yoon, C. S.; Oh, I.-H.; Sun, Y.-K. *J. Electrochem. Soc.* **2004**, *151*, A1911.

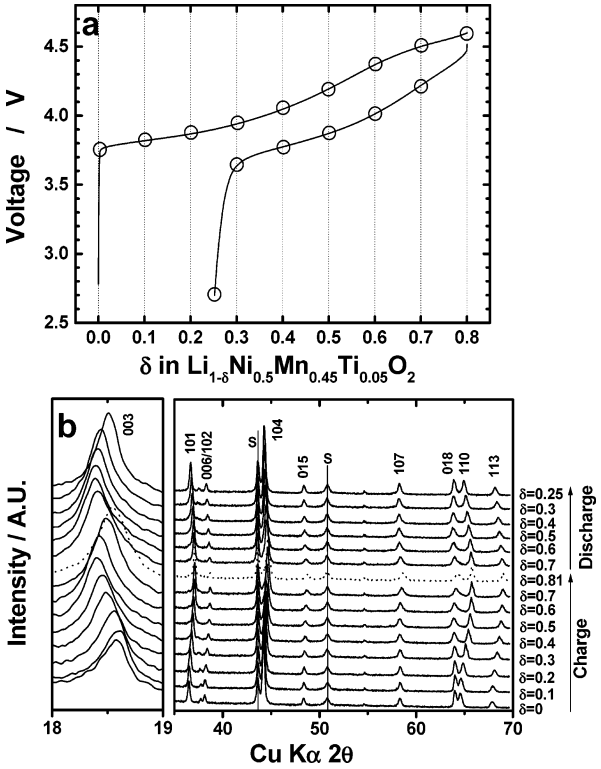

Figure 10. (a) Charge and discharge curves of the initial cycle for Li/$LiNi_{0.5}Mn_{0.5}O_2$ cell and (b) in situ XRD patterns of $Li_{1-\delta}Ni_{0.5}Mn_{0.45}Ti_{0.05}O_2$ as a function of Li content during the first cycle.

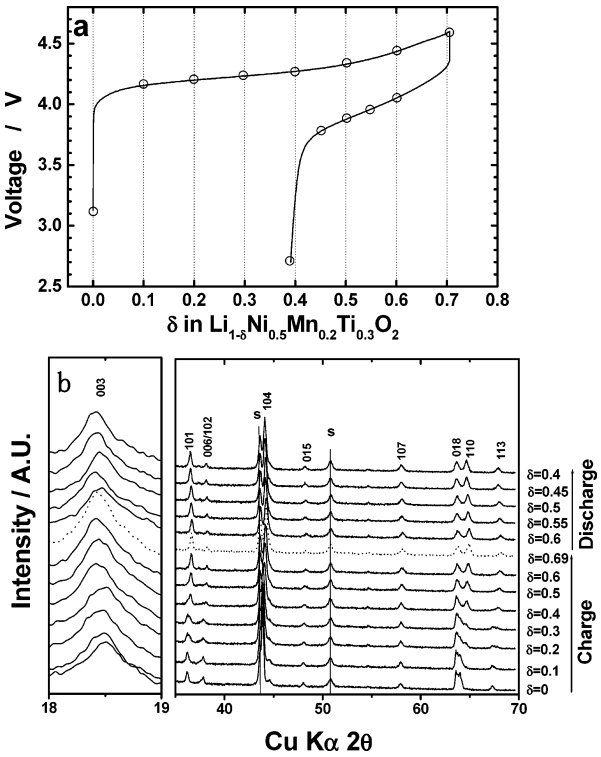

Figure 11. (a) Charge and discharge curves of the initial cycle for Li/$LiNi_{0.5}Mn_{0.5}O_2$ cell and (b) in situ XRD patterns of $Li_{1-\delta}Ni_{0.5}Mn_{0.2}Ti_{0.3}O_2$ as a function of Li content during the first cycle.

the increase in covalency between transition metal and oxygen bond. Similar variations were also observed in layered O3 type $LiCo_{0.5}Ni_{0.5}O_2$,[35] $LiNi_{1-x}M_xO_2$ (M = Mn, Mg),[36,37] and $LiMn_xCr_{1-x}O_2$.[23]

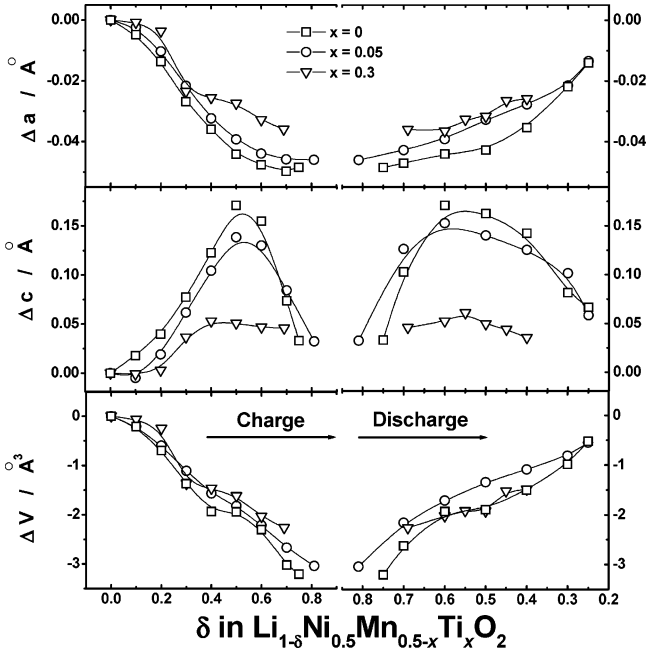

Figure 12. Variation in lattice parameters and unit cell volume of $Li_{1-\delta}Ni_{0.5}Mn_{0.5-x}Ti_xO_2$ ($x = 0$, 0.05, and 0.3).

On the other hand, a small amount of Ti substitution for Mn sites gave rise to somewhat smaller variation in the *c*-axis ($\Delta c = 0.05$ Å) for $Li_{1-\delta}Ni_{0.5}Mn_{0.45}Ti_{0.05}O_2$ probably due to the improved structural integrity by Ti doping in the crystal structure, compared to $Li_{1-\delta}Ni_{0.5}Mn_{0.5}O_2$ (Figure 12). Therefore, $LiNi_{0.5}Mn_{0.5-x}Ti_xO_2$ ($x = 0.05$ and 0.1) had the best cyclability among the samples in Figure 8, which would be ascribed to the reduced cation mixing of the host structure. A higher level of Ti substitution, $LiNi_{0.5}Mn_{0.2}Ti_{0.3}O_2$, showed a significantly suppressed variation in the *c*-axis during the first charge and discharge. The change in the *a*-axis clearly indicates that continuous oxidation of Ni^{2+} to Ni^{4+} is predominant in the first charge for $LiNi_{0.5}Mn_{0.2}Ti_{0.3}O_2$; a similar variation was observed for $LiNi_{0.5}Mn_{0.5-x}Ti_xO_2$ ($x = 0$, 0.05). In this case, it is possible that the severe cation mixing affected the variation in the *c*-axis. From these results, it is reasonable to think that incorporation of Ti ingredient into the host $LiNi_{0.5}Mn_{0.5}O_2$ structure brings about the improvement in structural integrity with the stronger bond of Ti−O and it consequently influences the *c*-axis variation and rechargeable capacity during cycling.

Figure 13 shows chemical Li^+ diffusion of $Li_{1-\delta}Ni_{0.5}Mn_{0.5-x}Ti_xO_2$ ($x = 0-0.3$) as a function of Li amounts. Chemical diffusivity was calculated for $x = Li_{1-\delta}Ni_{0.5}Mn_{0.5-x}Ti_xO_2$ ($x = 0-0.3$). $\tilde{D}_{Li^+}$ was calculated according to eq 1 derived by Huggins,[38]

$$\tilde{D}_{Li^+} = \frac{4}{\pi}\left(\frac{V_m}{FA}\right)^2\left[\frac{I^0\left(\frac{d\epsilon}{d\delta}\right)}{\left(\frac{d\epsilon}{dt^{1/2}}\right)}\right]^2 \text{ for } t \ll \frac{\left(\frac{d}{2\pi}\right)^2}{\tilde{D}_{Li^+}} \qquad (1)$$

(35) Ohzuku, T.; Ueda, A. *J. Electrochem. Soc.* **1994**, *141*, 2010.
(36) Yoshio, M.; Todorov, Y.; Yamato, K.; Noguchi, H.; Itoh, J.; Okada, M.; Mouri, T. *J. Power Sources* **1998**, *74*, 46.
(37) Pouillerie, C.; Croguennec, L.; Biensan, Ph.; Willmann, P.; Delmas, C. *J. Electrochem. Soc.* **2000**, *147*, 2061.
(38) Weppner, W.; Huggins, R. A. *J. Electrochem. Soc.* **1977**, *124*, 1569.

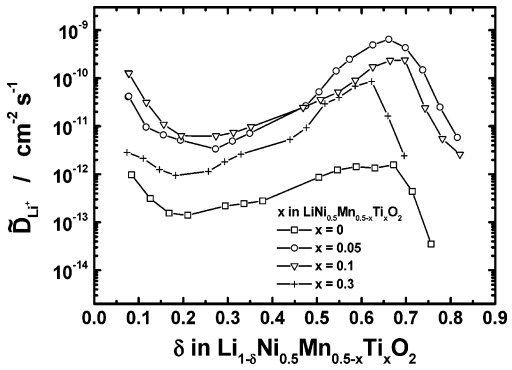

Figure 13. Chemical diffusion coefficient, $\tilde{D}_{Li^+}$, of $Li_{1-\delta}Ni_{0.5}Mn_{0.5-x}Ti_xO_2$ ($x = 0$, 0.05, 0.1, and 0.3) as a function of Li content.

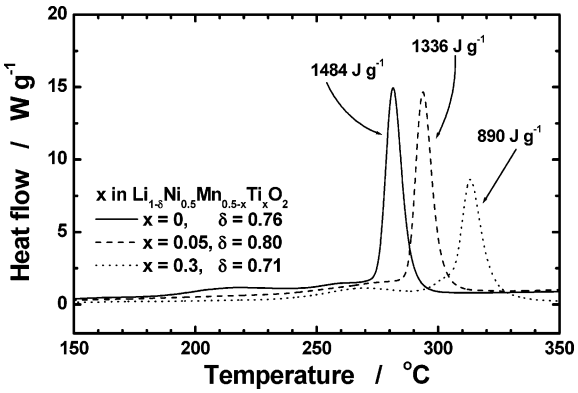

Figure 14. DSC traces of the $Li/LiNi_{0.5}Mn_{0.5-x}Ti_xO_2$ ($x = 0-0.3$) cells at 4.6 V.

where V_m is the molar volume, F is the faraday constant, A is the contact area between electrolyte and sample, I^0 is the applied constant electric current, $\{d\epsilon\}/\{d\delta\}$ is the slope of the coulometric titration curve which $\{d\epsilon\}/\{dt\}^{1/2}$ is the slope of the short-time transient voltage charge. The equation is valid for time shorter than the diffusion, $(d/2\pi)^2/\tilde{D}_{Li^+}$, where d is the average diameter of the grains. The $\tilde{D}_{Li^+}$ values derived from eq 1 are based on the following assumption: the molar volume (V_m) remains unchanged with the change in Li content in the compounds, and a single-phase reaction occurred. At first, $\tilde{D}_{Li^+}$ decreased from $\delta = 0$ to 0.2 or 0.4 in $Li_{1-\delta}Ni_{0.5}Mn_{0.5-x}Ti_xO_2$ ($x = 0-0.3$) as Li^+ intercalation proceeded for all compositions in Figure 13. The reason for the slight decrease in diffusivity in this range is not clear at present. The observed minimum in diffusivity coincides with the plateau observed in the voltage profile during the first charge in Figures 7, 9a, 10a, and 11a. A similar minimum in the $\tilde{D}_{Li^+}$ versus voltage plots is commonly observed in cathode materials which show a phase transition or some order−disorder transition during Li^+ de-/intercalation.[39,40] Then the diffusion coefficient began to increase to $\delta = 0.5-0.65$ in $Li_{1-\delta}Ni_{0.5}Mn_{0.5-x}Ti_xO_2$ ($x = 0-0.3$), after which the diffusion became slow again for all compositions in Figure 13. Changes in diffusion coefficients from $\delta = 0.3$ or 0.4 in $Li_{1-\delta}Ni_{0.5}Mn_{0.5-x}Ti_xO_2$ (Figure 13) could relate to the variation in the *c*-axis in Figure 12. It is likely that the variation in the diffusion coefficient would be influenced by the changes in *c*-axis which corresponds to the Li^+ diffusion interlayer space.

Ti-free $Li_{1-\delta}Ni_{0.5}Mn_{0.5}O_2$ exhibited a diffusion coefficient of about $10^{-13}\sim10^{-14}$ S cm^{-1}, for which the diffusion rate is quite lower than other transition metal oxides, such as $LiCoO_2$,[39,40] $LiNi_{1/3}Co_{1/3}Mn_{1/3}O_2$,[41] and $LiMn_2O_4$.[42] However, a small amount of Ti substitution $LiNi_{0.5}Mn_{0.5-x}Ti_xO_2$ ($x = 0.05$, 0.1) had a significantly improved chemical diffusivity of about $10^{-11}\sim10^{-12}$ S cm^{-1}, compared to $LiNi_{0.5}Mn_{0.5}O_2$ in Figure 13. The diffusion coefficient was still higher than $LiNi_{0.5}Mn_{0.5}O_2$, probably due to the larger interlayer distance (or Li−O bond length) of $LiNi_{0.5}Mn_{0.5-x}Ti_xO_2$ (Table 3). On the other hand, O3 type layered material always encounters cation mixing, especially Ni-based layered material as mentioned above. As a result, Ni^{2+} located at Li sites deteriorates Li^+ diffusion in the structure. As mentioned in Figure 4, the Ti doping to $LiNi_{0.5}Mn_{0.5}O_2$ led to significant lowering of the cation mixing. From this point of view, one can clearly see that such a lower cation mixing in the host structure brings about much higher Li^+ diffusion.

Figure 14 shows DSC results for electrodes of $Li_{1-\delta}Ni_{0.5}Mn_{0.5-x}Ti_xO_2$ ($x = 0-0.3$) charged to 4.6 V. The DSC experiments were made in welded scaled stainless steel tubes so that no leaking of pressurized electrolyte is possible. All materials exhibited simple DSC curves with onset temperatures of exothermic reactions higher than 270 °C. Thermal stability of the charged cathode material in the electrolyte increased gradually with increasing Ti doping amount. The $Li_{0.24}Ni_{0.5}Mn_{0.5}O_2$ exhibited a large peak between 275 and 295 °C, and it produced 1484 J g^{-1} of heat. Though a larger amount of Li^+ was extracted from $LiNi_{0.5}Mn_{0.45}Ti_{0.05}O_2$, compared with that from Ti-free sample, the generated heat was slightly decreased (1336 J g^{-1}) and the main exothermic temperature was shifted toward higher temperature of about 15 °C, which resulted from the improved structural integrity by Ti doping. $Li_{0.29}Ni_{0.5}Mn_{0.2}Ti_{0.3}O_2$ had a relatively small peak between 310 and 325 °C; also it only produced 890 J g^{-1} of heat. Hence, Ti substitution brought about the depression of the significant exothermic activity and reduced the heat generation at a highly delithiated state. $LiNi_{0.5}Mn_{0.5}O_2$ is stable, but Ti incorporation into $LiNi_{0.5}Mn_{0.5}O_2$ gives further thermal stability at a highly oxidized state in an electrolyte. Additionally, the present $LiNi_{0.5}Mn_{0.5-x}Ti_xO_2$ ($x = 0-0.3$) materials have better thermal safety characteristics than $LiNiO_2$-based cathode material.[43]

Figure 15 exhibits charge and discharge curves at 55 °C. The applied current density was 20 mA g^{-1}. The higher capacity of about 200 mA h g^{-1} and its superior retention during 50 cycles (>98%) are also achieved even at elevated temperature, which is due to the contribution of improved structural stability by Ti doping. Compared with room-temperature cycling in Figure 8b, the obtained capacity was higher due to increased Li^+ mobility at 55 °C.

(39) Jang, Y.-I.; Neudecker, B. J.; Dudney, N. J. *Electrochem. Solid-State Lett.* **2001**, *4*, A71.
(40) Levi, M. D.; Salitra, G.; Markovsky, B.; Teller, H.; Aurbach, D.; Heider, U.; Heider, L. *J. Electrochem. Soc.* **1999**, *146*, 1279.
(41) Shaju, K. M.; Subba Rao, G. V.; Chowdari, B. V. R. *J. Electrochem. Soc.* **2004**, *151*, A1324.
(42) Bang, H. J.; Donepudi, V. S.; Prakash, J. *Electrochim. Acta* **2002**, *48*, 443.
(43) Cho, J.; Jung, H.; Park, Y.; Kim, G.; Lim, H. S. *J. Electrochem. Soc.* **2000**, *147*, 15.

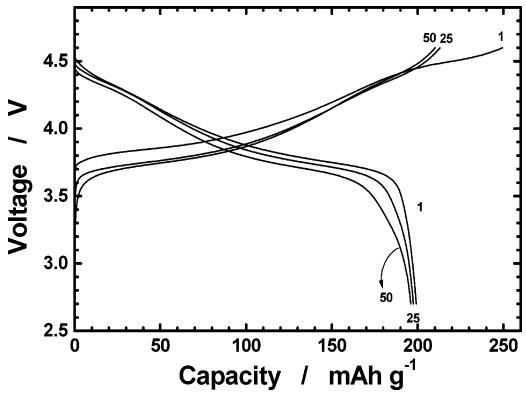

Figure 15. Charge and discharge curves of $Li/LiNi_{0.5}Mn_{0.45}Ti_{0.05}O_2$ cell. A constant current density of 20 mA g^{-1} was applied across the cathode between 2.7 and 4.6 V at 55 °C.

Conclusion

The layered oxides $LiNi_{0.5}Mn_{0.5-x}Ti_xO_2$ ($x = 0-0.3$) with the α-$NaFeO_2$ structure were synthesized by the emulsion drying method and the effect of Ti in $LiNi_{0.5}Mn_{0.5-x}Ti_xO_2$ on structure and electrochemical behaviors were investigated. A small amount of Ti doping gave rise to a decrease in cation mixing because the stronger Ti−O bond relative to Mn−O would stabilize the $LiNi_{0.5}Mn_{0.5}O_2$ structure, and a large amount of Ti substitution for Mn resulted in a higher degree of cation mixing and lower electronic conductivity. Electrochemical cycling of $Li/LiNi_{0.5}Mn_{0.5-x}Ti_xO_2$ ($x = 0-0.3$) cells were greatly dependent on the titanium doping. That is, $LiNi_{0.5}Mn_{0.5-x}Ti_xO_2$ ($x = 0.05, 0.1$) having a quite lower cation mixing delivered a higher capacity of about 175 mA h (g-oxide)$^{-1}$ and the retention was as high as 98% of its initial capacity at room temperature. The cycling results at 55 °C showed a much higher capacity of about 200 mA h (g-oxide)$^{-1}$ and good capacity retention (~98%). In situ XRD studies also indicated that incorporation of Ti ingredient into the host $LiNi_{0.5}Mn_{0.5}O_2$ structure brought about fewer changes in the *c*-axis during charge and discharge due to the structural stabilization by a stronger bond of Ti−O and it consequently influenced cycling performances and good thermal safety characteristics at a highly oxidized state. The improved physical properties also significantly enhanced chemical diffusivity of Li^+ by a small amount of Ti doping.

Acknowledgment. The authors thank Mr. S. Takahashi, Ms. A. Ueyama, and Ms. Y. Fujisawa for their helpful assistance in the experimental work. This study was financially supported by the program in ′00−′04 "Development of Rechargeable Lithium Battery with High Energy/Power Density for Vehicle Power Sources" of the Industrial Technology Research Grant Program from the New Energy and Industrial Technology Development Organization (NEDO), Japan.

CM050033J